

Crystal chemistry, superconductivity and magnetism in iron chalcogenides

E. GIANNINI^{1*}, R. VIENNOIS¹, R. ČERNÝ², M. HANFLAND³

¹ *Département de Physique de la Matière Condensée, Université de Genève,
24 Quai Ernest-Ansermet, CH-1211 Geneva, Switzerland*

² *Laboratoire de Crystallographie, Université de Genève,
24 Quai Ernest-Ansermet, CH-1211 Geneva, Switzerland*

³ *European Synchrotron Radiation Facility (ESRF),
6 Rue Jules Horowitz, BP 220, F-38043 Grenoble Cedex, France*

* *Corresponding author: Tel. +41-22-3796076; fax +41-22-3793502; e-mail: enrico.giannini@unige.ch*

Received July 2, 2010; accepted October 29, 2010; available on-line February 15, 2011

The structural simplicity of FeCh (Ch = S, Se, Te), in which the conducting layers are not separated by any third-atom layers, offers the best tool for investigating the nature of superconductivity and magnetism in Fe-based compounds. Either the pressure or the chemical composition distort the FeCh₄ tetrahedron and tune the electronic properties. When partially substituting Se for Te in the antiferromagnetic Fe_{1+x}Te, the excess of Fe is reduced and superconductivity appears over a wide range of compositions. Both the Fe excess and the Se substitution affect the structure and must be kept under control for tuning the structure deformation and the electronic properties. The excess of Fe stretches the FeCh₄ tetrahedron, thus inducing spin and charge localization. Below a critical Fe-Ch distance, the antiferromagnetism is weakened and superconductivity occurs, mediated by spin fluctuations as in the similar families of Fe-based oxy-pnictides. Uniaxial rather than hydrostatic pressure has a strong effect on the magnetic and superconducting properties of FeCh.

Fe-based superconductors / Fe chalcogenides / Magnetism and superconductivity

Introduction

The most simple system, among the various families of the recently discovered Fe-based superconducting pnictides and chalcogenides [1], is that of binary Fe-chalcogenides FeCh (Ch = S, Se, Te) [2-4]. These chalcogenides crystallize in the PbO-type structure, in which the Fe atoms are in a planar square lattice and tetrahedrally coordinated to four chalcogen atoms, thus forming layers of corner sharing FeCh₄ tetrahedra [5-7]. These layers are identical to those of FeAs₄ in all families of superconducting ferro-pnictides (see [1] and references therein), and therefore all the new Fe-based superconductors have in common the same structural core. However, superconducting Fe-chalcogenides and Fe-pnictides exhibit rather different behaviors upon chemical doping, as well as under pressure, and more accurate investigations on the structural details are needed to understand how do structural peculiarities drive their physical properties. Superconductivity occurs upon either aliovalent or isovalent doping, as well as upon applying pressure, and crystal chemistry seems to be more important than charge carrier doping in these materials. Even though

superconductivity in FeSe is dramatically dependent on pressure, rising up to $T_c = 37$ K at 9 GPa [8], FeTe does not exhibit any superconducting transition under pressures up to 19 GPa [9]. The end-compounds of the solid solution Fe(Te,Se) are substantially different from each other. The antiferromagnetic (AFM) ground state of the parent non-superconducting FeTe compound is theoretically predicted [10] and experimentally confirmed [11] to be different from that of the Fe-pnictide LaOFeAs. However, both the doped superconducting compounds, Fe(Te,Se) and La(O,F)FeAs, exhibit similar spin resonance at (π, π) [12,13], thus suggesting a common origin for superconductivity in iron chalcogenides and pnictides. A large effort has been devoted worldwide in the last two years to these new puzzling materials, and the experimental literature has recently been reviewed by Johnston [14].

In the present article, we will focus on the solid solution Fe_{1+x}Te_{1-y}Se_y and will discuss the effect of the chemical composition on its structure and physical properties. Based on our recent studies on single crystals of various compositions of Fe_{1+x}Te_{1-y}Se_y, we provide the evidence that the excess of Fe x and

Table 1 Parameters of the structure refinement for single crystals of $\text{Fe}_{1+x}\text{Te}_{1-y}\text{Se}_y$.

Nominal composition	FeTe	$\text{FeTe}_{0.8}\text{Se}_{0.2}$	$\text{FeTe}_{0.7}\text{Se}_{0.3}$	$\text{Fe}_{0.9}\text{Te}_{0.8}\text{Se}_{0.2}$	$\text{Fe}_{0.9}\text{Te}_{0.7}\text{Se}_{0.3}$
y [refined atomic fraction of Se]	0	0.21(4)	0.27(4)	0.22(4)	0.32(3)
x [refined excess of Fe]	0.087(3)	0.049(9)	0.053(9)	0.035(6)	0.013(9)
Space group	$P4/nmm$				
a [Å]	3.826(1)	3.815(2)	3.807(3)	3.806(3)	3.803(2)
c [Å]	6.273(3)	6.187(4)	6.153(7)	6.187(6)	6.136(3)
V [Å ³]	91.81(5)	90.02(9)	89.2(1)	89.6(1)	88.73(8)
Z	2				
Wavelength [Å]	0.71073 (Mo $K\alpha$)				
R_{int}	0.028	0.057	0.107	0.049	0.039
R_F	0.017	0.064	0.068	0.064	0.043
R_{wF}^2	0.031	0.156	0.159	0.169	0.098

the amount of Se doping y cooperate in determining the properties of these materials and both have to be taken under control. As a consequence, the magnetic and superconducting phase diagram of $\text{Fe}_{1+x}\text{Te}_{1-y}\text{Se}_y$ has to be drawn in 3D, rather than in 2D (T vs. Se fraction y) as commonly done. The excess of Fe in $\text{Fe}_{1+x}\text{Te}_{1-y}\text{Se}_y$ has a direct influence on the Fe-to-Te plane distance, which in turn determines the magnetic ground state at high temperature and can induce superconductivity at low temperatures, below a critical Fe-to-Te plane distance, equal to 1.72 Å. Preliminary high pressure diffraction studies are presented as well, and show that uniaxial pressure, rather than hydrostatic, is likely to provoke the structural changes that favor superconductivity in undoped Fe_{1+x}Te .

1. Structural studies

Single crystals of $\text{Fe}_{1+x}\text{Te}_{1-y}\text{Se}_y$ have been grown starting from two different Fe:(Te,Se) ratios, 1:1 and 0.9:1, and Se doping ranging from $y = 0$ to $y = 0.45$. The details of the sample processing and crystal growth are reported elsewhere [15]. Polycrystalline FeSe_{1-y} was also prepared by solid state reaction, for comparison. Particular care was taken during the sample preparation in order to avoid any precipitation of magnetic iron and iron oxides. Crystals with no or very low composition gradient ($\Delta y \leq 0.04$, as measured by Energy Dispersive X-ray spectroscopy (EDX)) were selected and used for this study. Small crystals (of the order of $0.1 \times 0.1 \times 0.01 \text{ mm}^3$) of selected compositions (see Table 1) were cleaved and used for single crystal X-ray diffraction (XRD) at room temperature in a Stoe IPDS II diffractometer, with Mo $K\alpha$ radiation, $\lambda = 0.71073 \text{ Å}$. The structure refinement was carried out by the least-squares method based on $|F|^2$ values using the SHELX-L program [16]. FeTe and FeSe are isomorphous and

crystallize in the same tetragonal PbO-type structure (the β -phase). Both are off-stoichiometric, but whereas the off-stoichiometry in FeSe_{1-y} is preferably ascribed to Se-deficiency [17,18], in Fe_{1+x}Te excess Fe atoms occupy an additional site in the Fe-Te plane [19-21]. The structure model was confirmed to be of the Cu_2Sb structure type, in the space group $P4/nmm$, according to which an additional site in the Te-plane can accommodate the Fe atoms (1-10%). The XRD data acquisition and structure refinement parameters are summarized in Table 1. A complete summary of the crystallographic parameters including atomic coordinates, displacement parameters, and refinement details, is reported in [15]. Being the atomic fraction of Se quite small in some cases, the atomic position of Se was constrained to that of Te, contrary to what was done by other authors [22].

Both the lattice parameters a and c decrease linearly with increasing Se doping in the Te-rich region, as shown in Fig. 1. The decrease of the c -axis length causes vertical shrinking of the FeTe_4 tetrahedron, with a consequent reduction of the vertical distance h of the Fe1 atom to the Te-plane (see inset of Fig. 1), and a weak tendency of the tetrahedral angles to approach the ideal value (109.47°). The relationship between both Se doping and Fe excess and the h vertical distance is shown in Fig. 2. In order to better show the mutual effect of both composition parameters on the structure, increasing x and decreasing y are plotted versus h . The first striking evidence coming out from Table 1 and Fig. 2 is that the excess of Fe and the fraction of Se are influencing each other. When starting from two Fe nominal contents (Fe:Ch = 1:1 and 0.9:1) at a fixed Se fraction, or from three Se nominal fractions ($y = 0, 0.2$ and 0.3) at a fixed nominal Fe content, we obtained different refined compositions of the final samples. In particular, the Fe excess decreases when the Se content increases. The decrease of the distance h as a

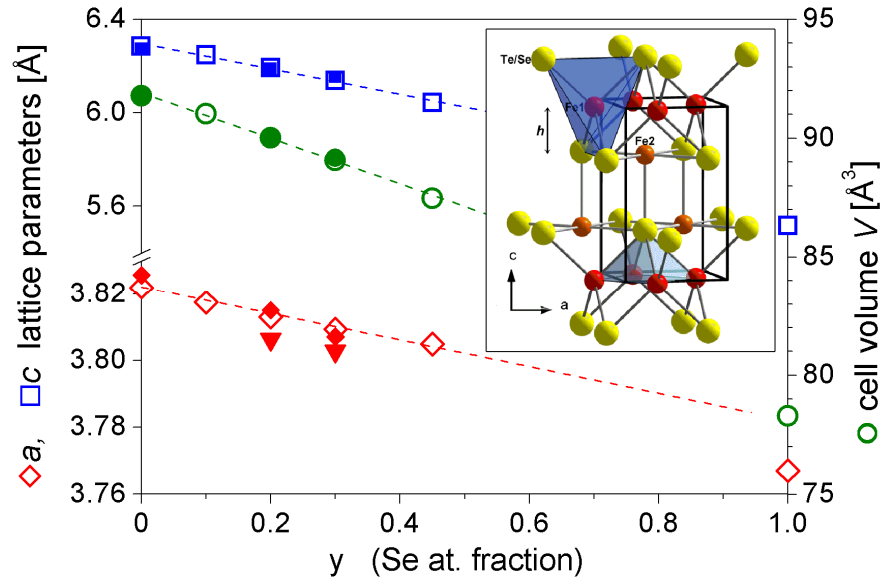


Fig. 1 Lattice parameters a (red rhombs), c (blue squares), and cell volume (green circles) as a function of the Se fraction y in $\text{Fe}_{1+x}\text{Te}_{1-y}\text{Se}_y$. Full symbols: single crystal X-ray diffraction; open symbols: powder diffraction from ground crystals; rhombs (triangles) refer to high (low) nominal Fe content. The end compound FeSe_{1-y} does not follow the linear trend. The crystal structure of $\beta\text{-Fe}_{1+x}\text{Te}$ is shown in the inset, in which the FeTe_4 tetrahedron and the distance h from Fe1 to the next Te layer are shown.

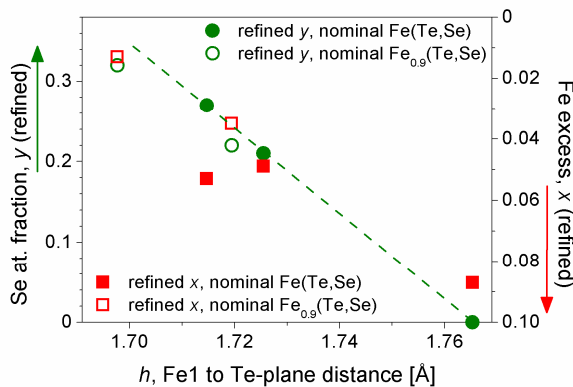


Fig. 2 The refined Fe excess (x , right axis) and Se content (y , left axis) are plotted vs. the vertical distance h . Full symbols refer to Fe-rich starting composition $\text{Fe}:\text{Ch} = 1:1$, open symbols to Fe-poor starting composition $\text{Fe}:\text{Ch} = 0.9:1$. The reduction of the starting Fe content favors a larger extent of Se substitutions and a larger reduction of the distance h . The dashed line is a guide for the eye.

function of the Se content is found to be more pronounced in samples with a lower Fe nominal content (open symbols in Fig. 2), corresponding to a lower excess of Fe obtained from structure refinements (see Table 1). The distance h depends on both x and y in an opposite way. This dependence is

clearly seen in Fig. 2, in which the plots of increasing y and decreasing x versus h show that both follow a similar linear trend.

2. Magnetic studies

The magnetic and superconducting behavior of the $\text{Fe}_{1+x}\text{Te}_{1-y}\text{Se}_y$ crystal was studied by means of DC magnetic susceptibility in a commercial SQUID magnetometer. $\chi(T)$ measurements were performed at high field (1 T) and low field (0.2 mT) for studying the magnetic and superconducting transition, respectively. The undoped parent compound Fe_{1+x}Te exhibits a Curie-Weiss-like behavior at high temperature and a sharp decrease of the susceptibility at $T = 67$ K corresponding to the structural (tetragonal to monoclinic) and magnetic (paramagnetic to AFM) transition, as previously observed and discussed by several authors [3,11,19,23]. The antiferromagnetic order observed in Fe_{1+x}Te takes place with a $(\pi, 0)$ propagation vector that is the diagonal direction of the Fe square sublattice [11]. This magnetic ground state of the parent compound is different from that of other Fe-based superconductors, namely “122” and “1111” pnictides, in which the propagation vector is directed along (π, π) [10,24]. The magnetostructural transition temperature is found to reduce when Se substitutes for Te, and vanish above $y = 0.4$ in crystals with the higher Fe nominal composition [15]. The Curie-Weiss-like behavior is maintained over the range of Se substitutions and is evidence of localized magnetic moments, but the $1/\chi(T)$ vs. T trend deviates more and

more from linearity upon Se substitutions [15]. In this series of samples, a broad bulk superconducting transition is only observed in samples with nominal composition $\text{FeTe}_{0.5}\text{Se}_{0.5}$, according to [20], even if evidence of surface superconductivity is found at lower Se content in transport measurements [25].

When crystals are grown starting from a lower Fe content in the nominal composition, the magnetic behavior is found to change drastically. The magnetic susceptibility becomes weakly dependent, or even independent, on temperature and exhibits a Pauli-like behavior that is evidence of itinerant magnetic moments. On the other hand, bulk superconductivity is observed at $y > 0.1$. Sharp superconducting transitions (~ 1 K) are measured in these crystals, up to a $T_{c,\text{max}} = 14$ K in $\text{Fe}_{0.9}\text{Te}_{0.55}\text{Se}_{0.45}$. Fig. 3 compares the magnetic susceptibility of two crystals with the same nominal Se content and two different Fe contents (see Table 1 for refined compositions). This shows unambiguously that the excess of Fe plays a major role in tuning not only the structural parameters, as discussed in the previous section, but also the magnetic and superconducting properties.

3. Phase diagram

The magnetic and superconducting behavior of these materials as a function of the chemical composition is commonly summarized in a 2-dimensional phase diagram in which either T_N (AFM order) or T_c (superconductivity) are plotted *versus* the nominal Se fraction y . In most cases, the reported phase diagrams present an intermediate region, at the transition from the AFM ground state to the superconducting one, in which signatures of both ground states are provided by several experimental techniques [26-28]. Based on the

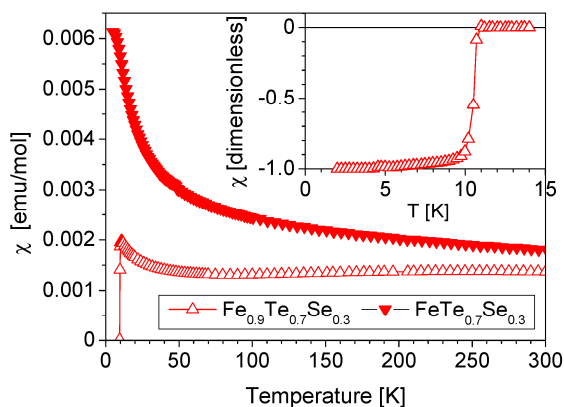


Fig. 3 Magnetic susceptibility (at $\mu_0 H = 1$ T) of two crystals with the same nominal Se content $y = 0.3$ but two different nominal Fe contents, Fe:Ch = 0.9:1 and 1:1. The magnetic behavior changes from Curie-like to Pauli-like paramagnetism upon reducing the excess of Fe. Moreover, bulk superconductivity occurs when the Fe content is reduced, as shown in the inset (transition measured at $\mu_0 H = 0.2$ mT).

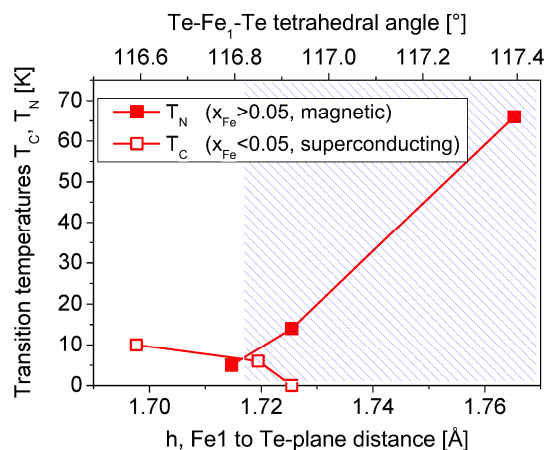


Fig. 4 AF and SC transition temperatures as a function of both the distance between Fe1 and the next Te-plane, and the tetrahedral angle. In the right hatched part, the material is antiferromagnetic (T_N given by full symbols). In the left part, at lower h distances and smaller angles, superconductivity occurs (T_c given by open symbols).

data presented in the previous sections, the key for driving the ground state from magnetic to superconducting in Fe-chalcogenides is likely to be the local symmetry around the Fe atoms in the square sublattice, rather than doping. For this reason, we draw a phase diagram in which the transition temperatures measured in our crystals (either T_N or T_c) are plotted as a function of the distance h . This is shown in Fig. 4 [15].

At a given distance $h = 1.72$ Å the system switches from an AFM ground state ($h > 1.72$ Å) to a SC one ($h < 1.72$ Å). This experimental observation is in excellent agreement with theoretical predictions based on Density Functional Theory calculations [29]. In that theoretical work, Moon and Choi found that the stability of the various magnetic states in $\text{FeTe}_{1-y}\text{Se}_y$ depends on h , and computed the total energy of the magnetic state as a function of h . They predicted a crossover from one magnetic ground state to another to occur around $h = 1.72$ Å, the value at which we measured the transition from the AFM to the SC ground state. The magnetic state predicted to be the most stable at $h > 1.72$ Å is a $(\pi, 0)$ double-stripe magnetic pattern, as observed in neutron diffraction experiments [11]. At $h < 1.72$ Å, the most stable magnetic order is found to be a (π, π) single-stripe magnetic pattern, as also found in other Fe-based superconducting pnictides [24].

According to our structural and magnetic study, such a crossover is driven by a structural modification induced by both a reduction of the Fe excess and an increase of the Se content. This closes the question about the apparent inconsistency between the Fermi Surface nesting scenario [30], common to

superconducting pnictides and chalcogenides, and the local moment interactions responsible for the peculiar magnetic state of Fe_{1+x}Te . The experimental evidences reported here, and the agreement with the theoretical predictions, reconcile Fe chalcogenides with Fe pnictides and confirm the possible common origin for superconducting pairing in these materials.

The importance of the chalcogen height h as the parameter that drives the ground state in these systems was already recognized by other authors [31]. However, tuning this parameter in Fe chalcogenides results from changing two composition parameters, instead of only one, and the correct representation of the phase diagram is therefore in 3 dimensions, $T_c(x,y)$, as reported in [15]. Local chemical inhomogeneities as well as a not well defined excess of Fe can widen and ill define the transition from the AFM to SC state.

4. High pressure studies

As a final comment on the effect of structural modifications on physical properties of Fe chalcogenides and pnictides, let's now consider the effect of pressure. Pressure is found to have a strong effect on magnetism and superconductivity in these materials (see the reviews [1,14] and references therein), and particularly in FeSe_{1-y} , in which T_c rises from 8 K to 37 K under 9 GPa [8]. However, undoped Fe_{1+x}Te does not exhibit any superconducting signal under pressures up to 19 GPa [9]. In order to elucidate the reason for such a difference between FeSe and FeTe, we have performed high-energy X-ray diffraction studies on pulverized crystals of $\text{Fe}_{1.087}\text{Te}$ under hydrostatic pressure up to 12 GPa, and compared the pressure effects to those of Se substitutions. High-pressure XRD experiments were performed at the ID09 beamline of the European Synchrotron Radiation Facility using monochromatic radiation ($\lambda = 0.414385 \text{ \AA}$) and diamond anvil cells with helium as pressure transmitting medium. The reduction of the lattice parameter a is found to be larger than upon Se substitutions ($a \sim 3.59 \text{ \AA}$ at $P = 10 \text{ GPa}$, $a \sim 3.80 \text{ \AA}$ at Se fraction $y = 0.5$), whereas the effect of mechanical and chemical pressure on the c -axis is comparable. The difference between the effect of the chemical pressure and that of hydrostatic mechanical pressure is shown in Fig. 5, in which the c/a ratio of the lattice parameters is plotted as a function of pressure (lower x -axis) and the Se fraction y (upper x -axis).

A stronger uniaxial pressure is exerted by the Se substitutions, whereas under hydrostatic pressure the unit cell is shrunk more isotropically. This difference could explain why pressure is not able to induce superconductivity in the undoped Fe_{1+x}Te . However, uniaxial pressure can act favorably for the superconductivity to occur. This is confirmed by the recent discovery of Han *et al.* [32], who succeeded in

growing superconducting Fe_{1+x}Te thin films under tensile strain, which causes an in-plane extension and out-of-plane contraction of the lattice, thus mimicking a uniaxial pressure.

The isothermal compressibility

$$\kappa_T = -(1/V)(\partial V/\partial P)$$

was calculated from the refinement of the high-pressure XRD patterns and the result is shown in Fig. 5 (red curve, right axis). The compressibility is found to decrease as a function of pressure from ~ 0.20 to $\sim 0.10 \cdot 10^{-10} \text{ Pa}^{-1}$ in the range 0-10 GPa.

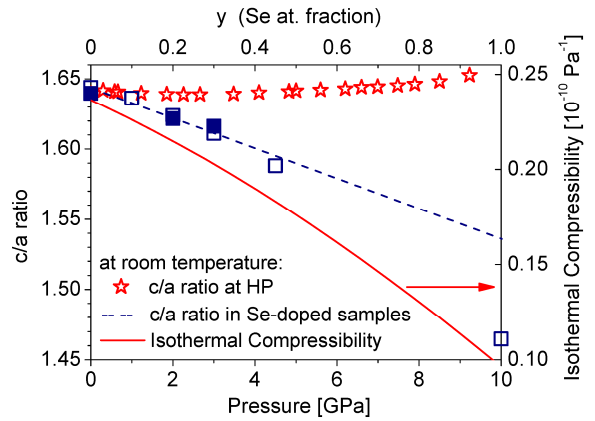


Fig. 5 Effect of hydrostatic mechanical pressure (red stars) and internal chemical pressure (blue squares and dashed guide line) on the lattice parameters of $\text{Fe}_{1.087}\text{Te}$. The blue symbols correspond to the same samples reported in Fig. 1. The isothermal compressibility is measured at room temperature and plotted as a function of pressure (red curve).

5. Conclusions

We have reported a systematic study of structural, magnetic and superconducting properties of the Te-rich solid solution $\text{Fe}_{1+x}\text{Te}_{1-y}\text{Se}_y$ based on single crystalline samples in which both the excess of Fe x and the Se fraction y are kept under control. Both composition parameters are found to influence the crystal structure and tune the vertical distance from the chalcogen atom to the next Fe-plane. The long-range commensurate anti-ferromagnetic (AFM) ground state is found to switch to the superconducting (SC) one at a given value of that distance, $h = 1.72 \text{ \AA}$, in good agreement with DFT calculation. The phase diagram of the Fe(Te,Se) system is more properly represented in 3 dimensions. High-pressure XRD has provided evidence that a strong uniaxial pressure effect is needed for softening the AFM order and favoring the SC state to take place. The isothermal compressibility of undoped $\text{Fe}_{1.087}\text{Te}$ is extracted from these measurements (at room T) and is of the order of $0.2 \cdot 10^{-10} \text{ Pa}^{-1}$.

References

- [1] K. Ishida, Y. Nakai, H. Hosono, *J. Phys. Soc. Jpn.* 78 (2009) 062001.
- [2] F.-C. Hsu, J.-Y. Luo, K.-W. Yeh, T.-K. Chen, T.-W. Huang, P.M. Wu, Y.-C. Lee, Y.-L. Huang, Y.-Y. Chu, D.-C. Yan, M.-K. Wu, *Proc. Natl. Acad. Sci. U.S.A.* 105 (2008) 14262.
- [3] K.-W. Yeh, T.-W. Huang, Y.-L. Huang, T.-K. Chen, F.C. Hsu, P.M. Wu, C. Lee, Y.-Y. Chu, C.-L. Chen, J.Y. Luo, Y.-D.-C. Yan, M.-K. Wu, *Eur. Phys. Lett.* 84 (2008) 37002.
- [4] Y. Mizuguchi, F. Tomioka, S. Tsuda, T. Yamaguchi, Y. Takano, *Appl. Phys. Lett.* 94 (2009) 012503.
- [5] G. Hägg, A.L. Kindström, *Z. Phys. Chem. B* 22 (1933) 453.
- [6] H. Haraldsen, F. Grønvold, J. Vihovde, *Tidsskrf. Kjem. Bergv.* 4 (1944) 96.
- [7] A.R. Lennie, S.A.T. Redfern, P.F. Schofield, D.J. Vaughn, *Mineral. Mag.* 59 (1995) 677.
- [8] S. Margadonna, Y. Takabayashi, Y. Oshishi, Y. Mizuguchi, Y. Takano, T. Kagayama, T. Nakagawa, M. Takata, K. Prassides, *Phys. Rev. B* 80 (2009) 064506.
- [9] H. Okada, H. Takahashi, Y. Mizuguchi, Y. Takano, H. Takahashi, *J. Phys. Soc. Jpn.* 78 (2009) 083709.
- [10] M.D. Johannes, I.I. Mazin, *Phys. Rev. B* 79 (2009) 220510(R).
- [11] W. Bao, Y. Qiu, Q. Huang, M.A. Green, P. Zajdel, M.R. Fitzsimmons, M. Zhernenkov, S. Chang, M. Fang, B. Qian, E.K. Vehstedt, J. Yang, H.M. Pham, L. Spinu, Z.Q. Mao, *Phys. Rev. Lett.* 102 (2009) 247001.
- [12] Y. Qiu, W. Bao, Y. Zhao, C. Broholm, V. Stanev, Z. Tesanovic, Y.C. Gasparovic, S. Chang, J. Hu, B. Qian, M. Fang, Z. Mao, *Phys. Rev. Lett.* 103 (2009) 067008.
- [13] M.D. Lumsden, A.D. Christianson, E.A. Goremychkin, S.E. Nagler, H.A. Mook, M.B. Stone, D.L. Abernathy, T. Guidi, G.J. MacDougall, C. de la Cruz, A.S. Sefat, M.A. McGuire, B.C. Sales, D. Mandrus, *Nat. Phys.* 6 (2010) 182.
- [14] D.C. Johnston, *arXiv:1005.4392* (unpublished).
- [15] R. Viennois, E. Giannini, D. van der Marel, R. Černý, *J. Solid State Chem.* 183 (2010) 769.
- [16] G.M. Sheldrick, SHELXL97 (1997), *Program for Crystal Structure Refinement*, University of Göttingen, Germany.
- [17] S. Margadonna, Y. Takabayashi, M.T. McDonald, K. Kasperkiewicz, Y. Mizuguchi, Y. Takano, A.N. Fitch, E. Suard, K. Prassides, *Chem. Commun.* (2008) 5607.
- [18] E. Pomjakushina, K. Conder, V. Pomjakushin, M. Bendele, R. Khasanov, *Phys. Rev. B* 80 (2009) 024517.
- [19] D. Fruchart, O. Convert, P. Wolfers, R. Madar, J.P. Senateur, R. Fruchart, *Mater. Res. Bull.* 10 (1975) 169.
- [20] B.C. Sales, A.S. Sefat, M.A. McGuire, R.Y. Jin, D. Mandrus, *Phys. Rev. B* 79 (2009) 094521.
- [21] T.J. Liu, X. Ke, B. Qian, J. Hu, D. Fobes, E.K. Vehstedt, H. Pham, J.H. Yang, M.H. Fang, L. Spinu, P. Schiffer, Y. Liu, Z.Q. Mao, *Phys. Rev. B* 80 (2009) 174509.
- [22] M. Tegel, C. Löhner, D. Johrendt, *Solid State Commun.* 150 (2010) 383.
- [23] M.H. Fang, H.M. Pham, B. Qian, T.J. Liu, E.K. Vehstedt, Y. Liu, L. Spinu, Z.Q. Mao, *Phys. Rev. B* 78 (2008) 224503.
- [24] C. de la Cruz, Q. Huang, J.W. Lynn, J. Li, W. Ratcliff II, J.L. Zarestky, H.A. Mook, G.F. Chen, J.L. Luo, N.L. Wang, P. Dai, *Nature* 453 (2008) 899.
- [25] I. Pallecchi, G. Lamura, M. Tropeano, M. Putti, R. Viennois, E. Giannini, D. van der Marel, *Phys. Rev. B* 80 (2009) 214511.
- [26] R. Khasanov, M. Bendele, A. Amato, P. Babkevich, A.T. Boothroyd, A. Cervellino, K. Conder, S.N. Gvasaliya, H. Keller, H.-H. Klauss, H. Luetkens, E. Pomjakushina, B. Roessli, *Phys. Rev. B* 80 (2009) 140511.
- [27] T.J. Liu, J. Hu, B. Qian, D. Fobes, Z.Q. Mao, W. Bao, M. Reehuis, S.A.J. Kimber, K. Prokes, S. Matas, D.N. Argyriou, A. Hiess, A. Rotaru, H. Pham, L. Spinu, Y. Qiu, V. Thampy, A.T. Savici, J.A. Rodriguez, C. Broholm, *arXiv:1003.5647* (unpublished).
- [28] N. Katayama, S. Ji, D. Louca, S.-H. Lee, M. Fujita, T.J. Sato, J.S. Wen, Z.J. Xu, G.D. Gu, G. Xu, Z.W. Lin, M. Enoki, S. Chang, K. Yamada, J.M. Tranquada, *arXiv:1003.4525* (unpublished).
- [29] C.-Y. Moon, H.J. Choi, *Phys. Rev. Lett.* 104 (2010) 057003.
- [30] A. Subedi, L. Zhang, D.J. Singh, M.H. Du, *Phys. Rev. B* 78 (2008) 134514.
- [31] Y. Mizuguchi, Y. Hara, K. Deguchi, S. Tsuda, T. Yamaguchi, K. Takeda, H. Kotegawa, H. Tou, Y. Takano, *Supercond. Sci. Technol.* 23 (2010) 054013.
- [32] Y. Han, W.Y. Li, L.X. Cao, X.Y. Wang, B. Xu, B.R. Zhao, Y.Q. Guo, J.L. Yang, *Phys. Rev. Lett.* 104 (2010) 017003.